Theoretical Investigations on the Structural Behavior of Biaxial Hollow Concrete Slabs

Prof. Dr. Nazar Kamel Ali Oukaili
Department of Civil Engineering
College of Engineering
Baghdad University
Email: dr_nazar12000@yahoo.com

Lect. Hassan Hamoudi Yasseen
Department of Civil Engineering
College of Engineering
Baghdad University
Email: hassanbayati@ymail.com

ABSTRACT

This paper presents a numerical analysis using ANSYS finite element program to simulate the reinforced concrete slabs with spherical voids. Six full-scale one way bubbled slabs of (3000mm) length with rectangular cross-sectional area of (460mm) width and (150mm) depth are tested as simply supported under two-concentrated load. The results of the finite element model are presented and compared with the experimental data of the tested slabs. Material nonlinearities due to cracking and crushing of concrete and yielding of reinforcement are considered. The general behavior of the finite element models represented by the load-deflection curves at midspan, crack pattern, ultimate load, load-concrete strain curves and failure modes shows good agreement with the experimental data.

Keywords: finite element analysis, one way slabs, prestressed concrete slabs, bubbled slabs, spherical voids.

تحريات نظرية على السلوك الانشائي للبلاطات الخرسانية المجوفة بمحورين

أ.د. نزار كامل علي العقيلي
قسم الهندسة المدنية
كلية الهندسة / جامعة بغداد

م. حسن حمودي ياسين
قسم الهندسة المدنية
كلية الهندسة / جامعة بغداد

الخلاصة

في هذا البحث تم استخدام التحليل العددي (طريقة العناصر المحددة ببرنامج ANSYS) لتمثيل البلاطات الخرسانية المسلحة ذات الفراغات الكروية الداخلية. تم تمثيل ستة بلاطات ذات الاتجاه الواحد بابعاد (٣٠٠٠ملم) طولا وذات مقطع مستطيل بابعاد (٤٦٠ملم) للعرض و(١٥٠ملم) للارتفاع. هذه البلاطات تم فحصها كبلاطات بسيطة الاسناد تحت نقطتي تحميل. تم استعراض النتائج النظرية ومقارنتها مع النتائج العملية للبلاطات المفحوصة. اخذ بنظر الاعتبار السلوك اللاخطي للمواد نتيجة لتشقق وسحق الخرسانة وخضوع حديد التسليح. اظهرت النتائج النظرية ان السلوك العام للنماذج المبنية بطريقة العناصر المحددة والمتمثلة بمنحي الحمل - الهطول عند منتصف العتبة، شكل التشققات، الحمل الاقصى، منحي الحمل- انفعال الخرسانة، وانماط الفشل، توافق جيدا مع النتائج العملية.

الكلمات الرئيسية: تحليل العناصر المحددة، البلاطات ذات الاتجاه الواحد، البلاطات الخرسانية المسبقة الشد، البلاطات المتفقعة، الفراغات الكروية.

1. INTRODUCTION

The wide application of the finite element method coupled with the availability of high-speed electronic digital computers has put the method in extensive use. Concrete structures may exhibit nonlinear behavior due to material or geometric nonlinearities. The material nonlinearity is due to cracking of concrete, crushing of concrete, yielding of reinforcement and nonlinear stress-strain response of concrete, while the geometric nonlinearity is caused when the structure experiences large deformations, **,ANSYS Help, 2009**.

Various attempt have been made in the past to reduce the weight of concrete slabs, without affecting their flexural strength. Not all the internal concrete can be replaced though, since aggregate interlock of the concrete is important for shear resistance, concrete in the top regions of the slab is necessary to form the compression block for flexural resistance, and concrete in the tension zones of the slab needs to bond with reinforcement to make the reinforcement effective for flexural resistance. Also the top and bottom faces of the slab need to be connected to work as a unit and insure the transfer the stresses, **,Marais, 2009.** The dominant advantage of slabs with internal spherical voids is that it uses (35%) less concrete than normal solid slabs. The plastic spheres replace the non-effective concrete in the centre of the section, Thus reducing the dead load of the structure by removing unused heavy material. Also leads to less structural steel since the need for reinforcement diminishes. The building foundations can be designed for smaller dead loads as well. On site construction time can be shortened since slabs with internal spherical voids can be precast, in relation to savings in material and time, cost reductions are also typical with this system as shown in **Fig.1**, **,BubbleDeck, Lighter Flat, 2006.**

2. EXPERIMENTAL PROGRAM

2.1 Characteristics of the Tested Slabs

Six full-scale one way structural concrete bubbled slabs of (3000mm) length with rectangular cross-sectional area of (460mm) width and (150mm) depth were tested as simply supported under two-concentrated loads, in which each specimens contain (80) plastic spheres of (100mm) diameter with ratio of (D/H=0.67) and (26.40%) reduction in self weight/m^3 as shown in **Fig. 2.** The variables studied are given in **Table.1 ,Oukaili, and Yasseen, 2014.** Load (P) is applied by means of hydraulic jack which acted on the slabs as two symmetrical concentrated loads (with ratio of shear span (a) to effective depth (d), a/d=6.88) (see **Fig. 3**). For all specimens, deflection at midspan, first cracking load, ultimate load and concrete strains are recorded and measured at various stages of loading.

2.2 Material Properties

The specimens constructed using a concrete with a compressive strength of approximately (40 MPa). The concrete produced in the laboratory using normal Portland cement, fine aggregate, and crushed coarse aggregate of (10mm) maximum nominal size. Seven-wire strand of (12.7mm) nominal diameter (grade 270, low relaxation, confirming to **ASTM A416/ A416M-06** used as

flexural reinforcement, at a prestressing level of (70%) of the ultimate strength (1860 MPa). In addition, different diameters (12mm, 10mm and 6mm) of steel bars used in this study as flexural and shear reinforcement. The plastic spheres were made by embodying high density polypropylene (HDPE) from recycled plastic with diameter (100mm).

3. FINITE ELEMENT ANALYSIS

3.1 Modeling of Material Properties

3.1.1 Concrete

The concrete is assumed to be homogeneous and initially isotropic. The compressive uniaxial stress strain relationship for the concrete model is obtained by using the following equations to compute the multilinear isotropic stress- strain curve for the concrete as shown in **Fig. 4, ,Desayi and Krishnan, 1964.**

$$f_c = E_c \varepsilon \qquad for\ 0 \le \varepsilon \le \varepsilon_1 \qquad \text{Eq. (1)}$$

$$f_c = \frac{E_c\,\varepsilon}{1+(\frac{\varepsilon}{\varepsilon_o})^2} \qquad for\ \varepsilon_1 \le \varepsilon \le \varepsilon_o \qquad \text{Eq. (2)}$$

$$f_c = f_c' \qquad for\ \varepsilon_o \le \varepsilon \le \varepsilon_{cu} \qquad \text{Eq. (3)}$$

$$\varepsilon_o = \frac{2f_c'}{E_c} \qquad \text{Eq. (4)}$$

The modulus of elasticity, E_c, can be calculated with a reasonable accuracy from the empirical formula, **ACI 318M-14**.

$$E_c = 0.043(w)^{1.5}(f_c')^{0.5}$$

For the normal weight concrete based on a dry unit weight (2200-2500 kg/m^3), E_c can be permitted to be taken as, **ACI 318M-14**.

$$E_c = 4700\sqrt{f_c'}$$

Poisson's ratio (v) of concrete has been observed to remain approximately constant and ranges from about (0.15 to 0.22) up to a stress level of 80% of f_c', **,Neville, 1987.**

3.1.2 Reinforcing Steel

Ordinary Reinforcement: For all practical purposes, steel exhibits the same stress-strain curve in compression as in tension. The steel stress-strain relation exhibits an initial linear elastic portion, a yield plateau, a strain hardening range in which stress again increases with strain and, finally, a range in which the stress drops off until fracture occurs. The extent of the yield plateau is a function of the tensile strength of steel. For computational convenience it even often suffices to idealize the one dimensional stress-strain relation for steel, as shown in **Fig. 5 ,Kwak, 1990.**

Prestressing Strands: The multi-linear curve option is useful to define stress-strain curve of prestressing strand elements. Coordinates for each point on the curve are derived using the equations available in **PCI Manual for the Design Handbook** (**PCI, 2010)** for low relaxation strands of grade (270 ksi) (1860 MPa) which have been summarized below and plotted in **Fig. 6**.

For the elastic segment of the curve when ($\varepsilon_p < 0.0085$), stress in the LINK8 element (f_p) is calculated from the following linear equation:

$$f_p = 28500\varepsilon_p \quad \text{(ksi)} \qquad \text{Eq. (5)}$$

While for the plastic segment ($\varepsilon_p > 0.0085$), the stress in strand elements (f_p) is calculated from the following expression:

$$f_p = 270 - \frac{0.04}{\varepsilon_p - 0.007} \quad \text{(ksi)} \qquad \text{Eq. (6)}$$

where f_p and ε_p are the strand stress and corresponding strain at any arbitrary point on the curve.

3.2 Element Types

SOLID65 is used for the 3-D modelling of solids with or without reinforcing bars (rebar). The solid is capable of cracking in tension and crushing in compression. The element is defined by eight nodes having three degrees of freedom at each node: translations of the nodes in x, y, and z-directions. This 8-node brick element is used, in this paper, to represent the concrete. The element is defined by the isotropic material properties. The geometry, node locations, and the coordinate system for this element are shown in **Fig. 7**.

LINK8 is a spar (or truss) element which used to model the steel reinforcement. The 3-D spar element is a uniaxial tension-compression element with three degrees of freedom at each node: translations of the nodes in x, y, and z-directions. The geometry, node locations, and the coordinate system for this element are shown in **Fig. 8**.

SOLID45 is defined with eight nodes having three degrees of freedom at each node; translations in x, y, and z directions. SOLID45 is used to model the steel plate which existed under point load (applied load) and supports in order to avoid stress concentration problems. The geometry, node locations, and the coordinate system for this element are shown in **Fig. 9 ,ANSYS Help, 2009.**

3.3 Real Constant and Material Properties

The real constants for all materials used in constructing the model of reinforced concrete bubbled slabs are described and listed in **Table. 2** Parameters needed to define the material models for the first specimen are given in **Table. 3**

3.4 Modeling of Bubbled Slab

ANSYS program create the solid slab, solid spheres, plates, and supports as volumes. By taking advantage of the symmetry of both slab geometry and loading, one quarter of the entire model slab is used for the element analysis. The model is (1500mm) in length, with a cross-section of (150mm

x 230mm) for solid slab. Due to symmetry, only one loading plate and support plate are needed. The loading and support plates are (230mmx 150 mm x 10mm). Twenty solid spheres with radius of (50mm) are created and moved to the correct positions inside the block of solid slab and by subtract command, subtracting all the solid spheres from the solid slab, the voids will be formed in the center of cross-section. The combined volumes of the slab, spheres, plates and supports, are shown in **Fig. 10**. LINK8 elements are used to create the upper and lower welded wire meshes of (3mm) diameter in addition to the flexural and shear reinforcement see **Fig. 11**.

3.5 Meshing of Bubbled Slab

Using of a triangular mesh with tetrahedron volume is necessary to obtain good results from the SOLID65 element. Therefore, the mesh is set up in such manner that triangular elements are created see **Fig. 12**. Also, the volume free command is used to mesh the steel plate and support. This properly sets the width and length of elements in the plates to be consistent with the elements and nodes in the concrete portions of the model.

3.6 Loads and Boundary Conditions

Rollers are used to show the symmetry condition at the internal faces. Moreover, a single line support is placed under the centerline of the support position to allow rotation of the support while vertical movement is restricted; when the loaded slab starts to displace download, rotation of the support should be permitted. The single line of external forces is applied to the centerline of steel plate to reduce the stress concentration caused by the applied force and result in early cracking.

4. COMPARISON OF EXPERIMENTAL AND ANALYTICAL RESULTS

4.1 Load-deflection Relationship

Figures 14 through **17** show load-deflection curves of the bubbled slabs of the present finite element analysis and experimental results.

It can be observed that, the present finite element model performs satisfactorily and it predicts the real behavior of the bubbled slab. However, the finite element load-deflection curves in the linear stage are somewhat stiffer than the experimental responses for slab (BD1), while, the analytical load-deflection curves of slabs (BD2, BD4 and BD5) well match the test data. For bubbled slabs (BD6 and BD7), the finite element load-deflection curves in the linear stage are somewhat stiffer than that of the experimental responses. After first cracking, the stiffness of the modeled elements is slightly higher than that of the experimental specimens. There are several reasons that may cause the higher stiffness in the finite element models. First, micro-cracks produced by drying shrinkage and handling which are present in the concrete to some degree. They would reduce the stiffness of the actual specimens, while the finite element models do not include micro-cracks. Second, the perfect bond between the concrete and reinforcing steel is assumed in the finite element analysis, but the assumption would not be true for the actual specimens. As bond slip occurs, the composite action between the concrete and reinforcing steel begins to diminish. Thus, the overall stiffness of the actual specimens could be lower than what the finite element models predict, due to factors that are not incorporated into the models.

The load-deflection response at midspan for the bubbled slabs with prestress steel is essentially bilinear with a transition curve at the cracking load. This is due to the linear characteristics of the prestressing strands that do not show any yield plateau.

The contours representing the deflected shapes of the specimen BD7 due to prestressing force and ultimate load is shown in **Fig. 18**.

4.2 First Cracking and Ultimate Loads

The first cracking and ultimate loads obtained in analysis by (ANSYS) program are compared with experimental results for all the bubbled slabs. The values are given in **Table. 4**.

In finite element analysis, it is found that, the first cracking load (P_{cr}) is formed at (39.8%, 53%, 55.5%, 69%, 63% and 69.8%) of the ultimate load (P_u) of bubbled slabs (BD1, BD2, BD4, BD5, BD6 and BD7), respectively. Based on the finite element analysis, the first cracking loads for all models are almost higher than those from experimental results.

The average value of the ratio of the experimental load at first cracking to the corresponding load observed in the analytical results is found be (0.91) with a standard deviation of (0.084). While, at ultimate load, the average and the standard deviation become (0.95 and 0.073) respectively.

4.3 Load-Concrete Strain Relationship

Figures 19 and **20** show the distribution of concrete strains at the ultimate load in the longitudinal x-direction, along the bubbled slabs (BD1) and (BD4), respectively. It is noted that, the maximum compressive strains for (BD1) are at the upper fibers of the cross-section at midspan, while, for prestressed bubbled slab (BD4), they are located at the support region at the level of prestressing steel, this is due to the assumption of the perfect bond between the concrete and prestressing steel in the finite element analysis. But, the maximum tensile strains for all bubbled slabs are located in the region occupied by the spherical voids.

The compressive and tensile strains data for concrete collected from the experimental test of bubbled slabs are compared with the results obtained from the finite element analysis. It is noted that, the analytical load-concrete strain curves in the linear stage are somewhat stiffer than the experimental responses, after this stage, the strains in the concrete calculated by ANSYS are higher than those from the experimental results especially in the bottom fibers as shown in **figures 21** and **22**.

The analytical results show that, there is a significant increase in concrete strain of bubbled section occupied by the spherical voids in comparison with solid section (between two voids) for the bubbled slab.

4.4. Crack Pattern and Failure Mode

In finite element analysis, it is observed that, the first flexural cracking initiates at (39.8%-69%) of the ultimate load, and at this stage of loading, the tensile stress in concrete reaches the modulus of rupture, and crack appears in the zone of maximum tensile stress. As the load increases, flexural-shear cracks appear in shear span. Flexural failure mode for bubbled slab (BD1) is shown as circles

at midspan and spread toward the top fiber of bubbled slab in compression zone as shown in **Fig. 23**.

For prestressed bubbled slabs (BD2, BD4, BD5, BD6 and BD7), the first flexural cracks are observed as circles in the tension face of the bubbled slabs at midspan. As the load is increased, these cracks spread horizontally to the support and vertically to the top fiber of slabs, and when load increases, web-shear or flexural-shear cracks form diagonally in the voids region resulting in shear failure, as shown clearly in **Fig. 24** for bubbled slab (BD6).

5. CONCLUSION

Based on the analytical results, the following conclusion may be drawn:

1- The general behavior of the finite element models represented by the load-deflection curves at the midspan of the bubbled slabs shows good agreement with the experimental results. However, the finite element models show slightly more stiffness than the test data in both the linear and nonlinear ranges. The effects of bond slip and micro-cracks that occur in the experimental slabs which are excluded in the finite element models are contributing to the higher stiffness of the finite element models.

2- First cracking and ultimate loads for most models calculated by the finite element analysis are almost higher than those from the experimental data.

3- The variation of strain over the depth of cross-sections due to the incremental load for the finite element models, shows good agreement with the test data. Also, The analytical results show that, there is a significant increase in concrete strain of bubbled section occupied by the spherical voids in comparison with solid section (between two voids).

4- The crack patterns at the first cracking and ultimate loads obtained by the finite element models correlate well with the observed failure modes of the experimental slabs.

REFERENCES

- ACI Committee 318, 2014, "*Building Code Requirements for Structural Concrete (ACI 318M-14) and commentary",* American Concrete Institute, Farmington Hills, 524pp.
- ANSYS, 2005, "*ANSYS Help",* Release 10.0, Copyright.
- ASTM A416/ A416M, 2006, "*Standard Specification for Steel Strand, Uncoated Seven-Wire for Prestressed Concrete",* ASTM International.
- BubbleDeck, 2006, "*Lighter Flat Slab Structures with BubbleDeck* ،" www.BubbleDeck-UK.com.
- Desayi, P. and Krishnan, S.,1964, "*Equation for the Stress-Strain Curve of Concrete",* Journal of the American Concrete Institute, Vol. 61, No. 3, pp. 345-350.

- Kwak, H.G. and Filippou F.C., 1990, *"Finite Element Analysis of Reinforced Concrete Structures under Monotonic Loads"*, Report No. UCB/SEMM-90/14 Structural Engineering, Mechanics and Materials Department of Civil Engineering University of California.

- Marais, C. C., 2009, **"***Design Adjustment Factors and Economical Application of Concrete Flat-Slabs with Internal Spherical Voids in South Africa",* M.Sc Thesis, University of Pretoria.

- Neville, A.M., and Brooks, J.J., 1987, "*Concrete Technology",* Longman Scientific and Technical, U.K, 438 pp.

- Oukaili, N., and Yasseen, H., 2014, "*Effect of Prestressing Force on Performance of Polymer Bubbled Deck Slabs",* The 7th International Conference on FRP Composites in Civil Engineering (CICE 2014), Vancouver, Canada, pp. 1-6

- Precast/Prestressed Concrete Institute (PCI), 2010, **"***Design Handbook",* Sixth Edition,

- Precast/Prestressed Concrete Institute, Chicago, 736 pp.

NOMENCLATURE

Δ_u = ultimate deflection, mm

ε_{cu} = ultimate compressive strain

f_c' = the cylinder compressive strength of concrete, MPa

f_c = stress at any strain ε, MPa

ε_1 = strain corresponding to $(0.3f_c')$

ε_o = strain at the ultimate compressive strength f_c'

w_c = the air-dry unit weight of concrete, kg/m³

Table 1. Summary of Test Data, **,Oukaili and Yasseen, 2014.**

Specimen	Thickness of Specimen, mm	Sphere Diameter, mm	Distance c/c of Spheres, mm	D/H	Type of Reinforcement	Number of Bars and / or Strands	Number of Spheres
BD1	150	100	115	0.67	Non-prestressed	2φ12 mm	80
BD2	150	100	115	0.67	Partially Prestressed	2φ12 mm2φ12 mm	80
BD4	150	100	115	0.67	Partially Prestressed	2φ12 mm & 2φ12.7 mm	80
BD5	150	100	115	0.67	Fully Prestressed	2φ12 mm & 2φ12.7 mm	80
BD6	150	100	115	0.67	Partially Prestressed	2φ12 mm & 3φ12.7 mm	80
BD7	150	100	115	0.67	Fully Prestressed	3φ12.7 mm	80

Table 2. Real Constant.

Real constant set	Element type	Constant			
1	SOLID65		Real constant for Rebar 1	Real constant for Rebar 2	Real constant for Rebar 3
		Material number	0	0	0
		Volume ratio	0	0	0
		Orientation angle	0	0	0
2	LINK8	Cross-sectional area, mm	99.6	Strand Φ 12.7mm	
		Initial strain, mm/mm	0.0056		
3	LINK8	Cross-sectional area, mm	113.09	Steel Φ 12mm	
		Initial strain, mm/mm	0		
4	LINK8	Cross-sectional area, mm	78.53	Steel Φ 10mm	
		Initial strain, mm/mm	0		

5	**LINK8**	**Cross-sectional area, mm**	**7.06**	**Steel Φ 3mm**
		Initial strain, mm/mm	**0**	
6	**LINK8**	**Cross-sectional area, mm**	**28.27**	**Steel Φ 6mm**
		Initial strain, mm/mm	**0**	
7	**SOLID45**			**Steel Plate**

Table 3. Material Properties

Material model number	Element type	Material properties		
1	SOLID65	**Linear i otropic**		
		Ex	**27583MPa**	
		PRXY	**0.2**	
		Multilinear isotropic		
			Strain	**Stress, MPa**
		Point 1	**0.00046**	**12.93**
		Point 2	**0.0008**	**15.98**
		Point 3	**0.0015**	**29.74**
		Point 4	**0.0020**	**35.83**
		Point 5	**0.0029**	**43.10**
		Concrete		
		ShrCf-Op	**0.2**	
		ShrCf-Cl	**0.8**	
		UnTensSt	**4.31MPa**	
		UnCompSt	**43.1MPa**	
		BiCompSt	**0**	
		HydroPrs	**0**	
		BiCompSt	**0**	
		UnTensSt	**0**	
		TenCrFac	**0**	

Material model number	Element type	Material properties		
2	LINK8 Strand Φ 12.7mm	Linear isotropic		
		Ex	197500MPa	
		PRXY	0.3	
		Multilinear isotropic		
			Strain	Stress, MPa
		Point 1	0.0085	1657
		Point 2	0.009	1724
		Point 3	0.0095	1751
		Point 4	0.010	1770
		Point 5	0.015	1827
		Point 6	0.020	1860
3	LINK8 Steel Φ 12mm	Linear isotropic		
		Ex	200000MPa	
		PRXY	0.3	
		Bilinear isotropic		
		Yield Stss	442MPa	
		Tang Mod	0MPa	
4	LINK8 Steel Φ 10mm	Linear isotropic		
		Ex	200000MPa	
		PRXY	0.3	
		Bilinear isotropic		
		Yield Stss	483MPa	
		Tang Mod	0MPa	
5	LINK8 Steel Φ 3mm Meshes	Linear isotropic		
		Ex	200000MPa	
		PRXY	0.3	
		Bilinear isotropic		
		Yield Stss	546MPa	
		Tang Mod	0MPa	
6	LINK8 Steel Φ 6mm Stirrup	Linear isotropic		
		Ex	200000MPa	
		PRXY	0.3	
		Bilinear isotropic		
		Yield Stss	598MPa	
		Tang Mod	0MPa	

7	SOLID45	Linear isotropic	
		Ex	200000MPa
		PRXY	0.3

Table 4. Comparison of Experimental and Analytical Results.

Specimen	Experimental				Finite Element Analysis				$P_{cr}(EXP)/P_{cr}(FEM)$	$P_u(EXP)/P_u(FEM)$
	Camber, mm	P_{cr}, kN	P_u, kN	Δ_u, mm	Camber, mm	P_{cr}, kN	P_u, kN	Δ_u, mm		
BD1	0	14	43.5	14.90	0	16.5	41.5	13.84	0.85	1.05
BD2	2.16	54	92	21.54	2.00	56.5	106.5	18.97	0.95	0.86
BD4	2.30	46	86	20.00	2.00	51.5	92.75	19.75	0.89	0.92
BD5	2.45	40	78	16.05	2.10	51	73.87	17.42	0.78	1.05
BD6	3.98	65	98	19.42	3.00	66.5	105.25	16.66	0.97	0.93
BD7	4.40	61	94	14.60	3.40	66.5	95.25	13.49	0.91	0.98

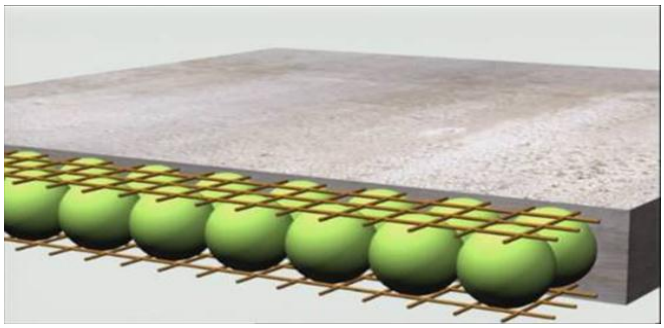

Figure 1. BubbleDeck floors system

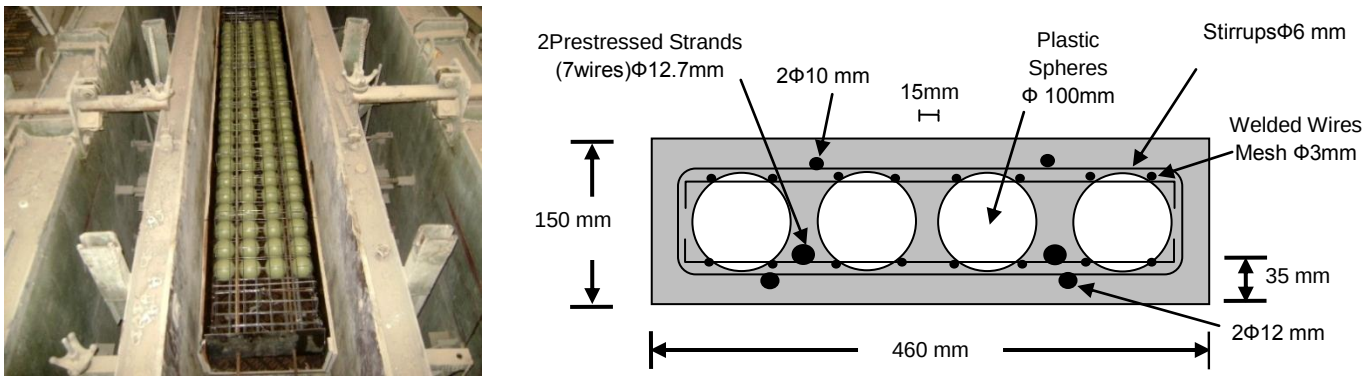

Figure 2. Reinforcement Details

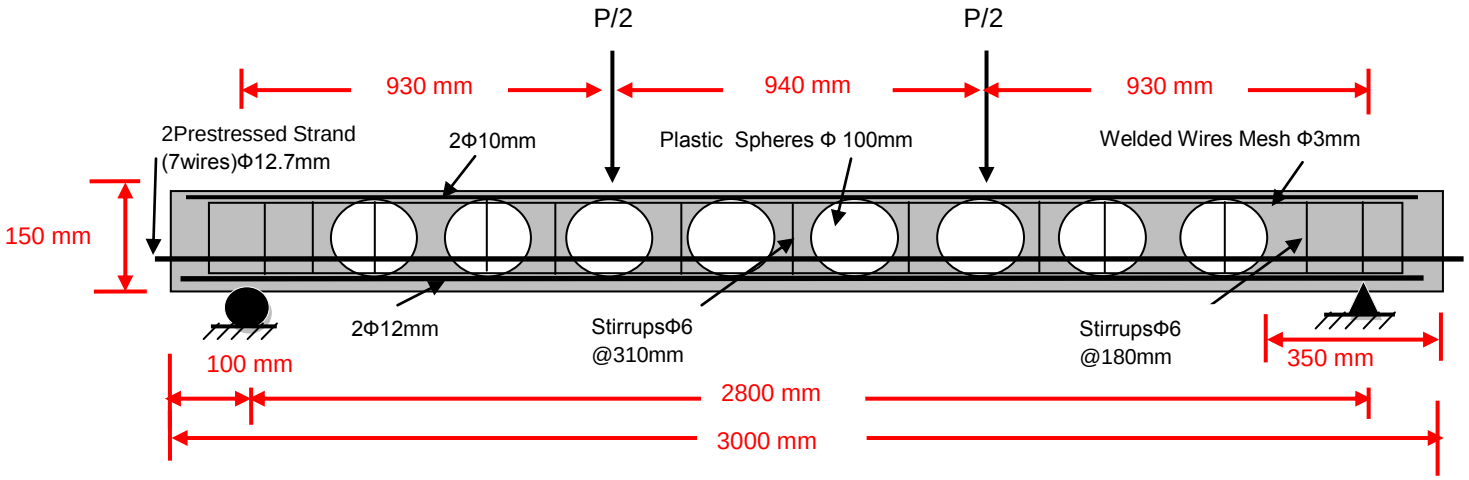

Figure 3. Full-Scale Model under loading

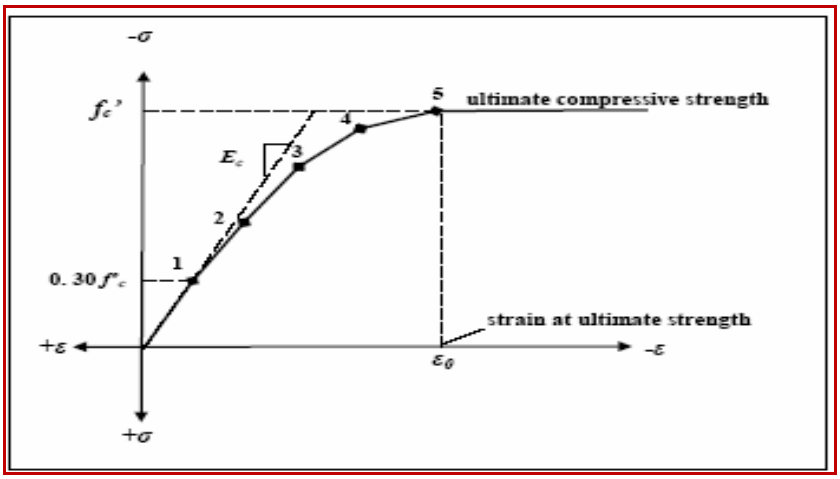

Figure 4. Simplified Compressive Uniaxial Stress-Strain Curve for Concrete

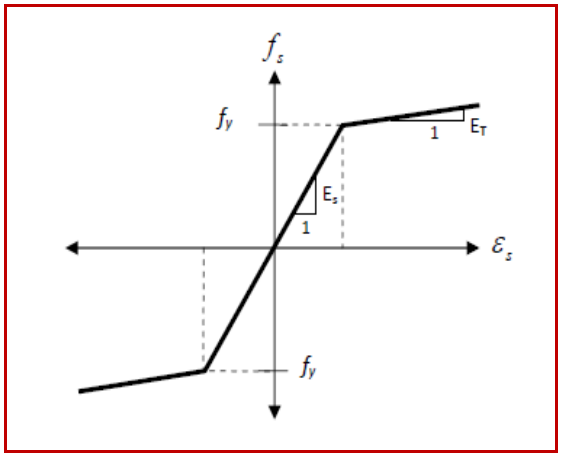

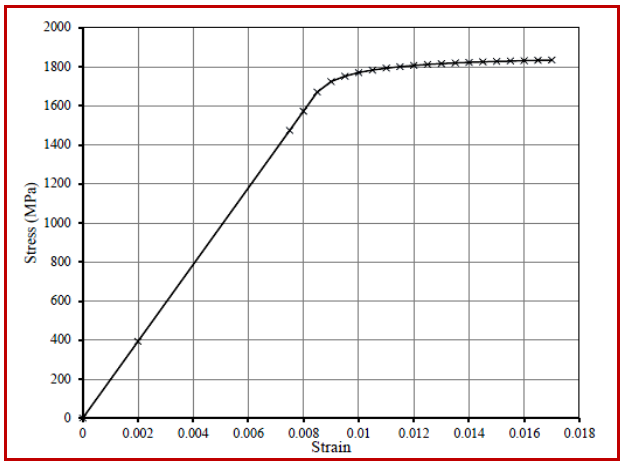

Figure 5. Steel Stress-Strain Relation

Figure 6. Stress-Strain Curve for Strand

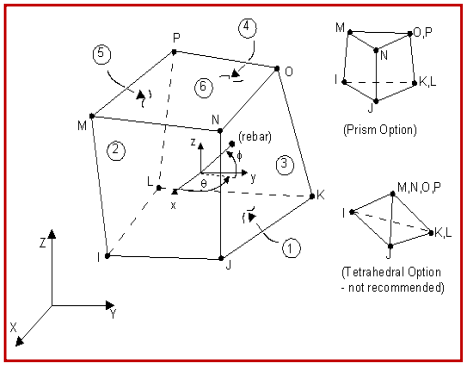

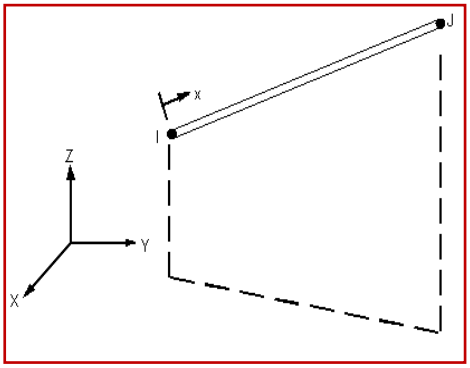

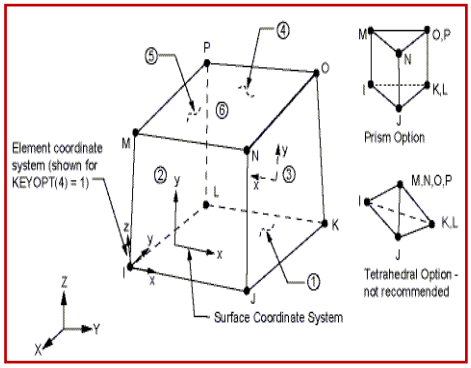

Figure7. SOLID65 Element **Figure 8.** LINK8 Element **Figure 9.** SOLID45 Element

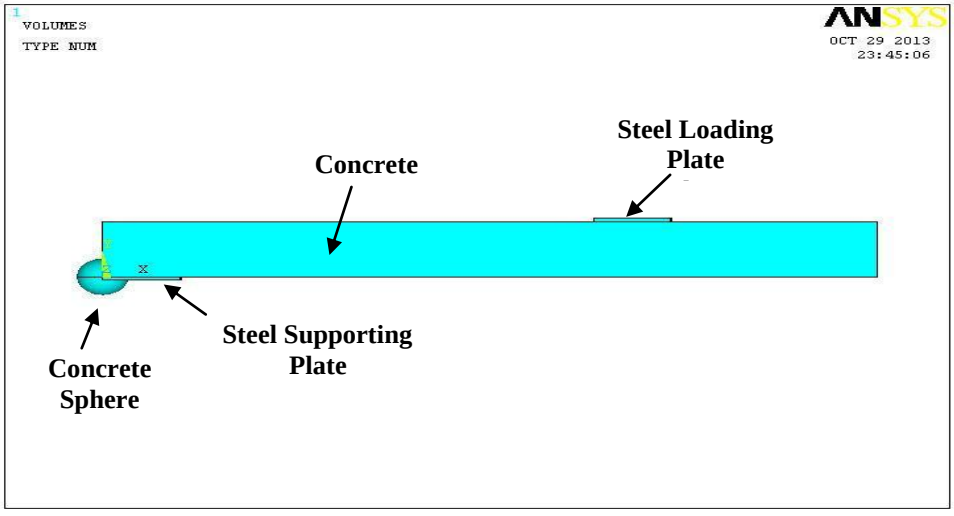

Figure 10. Modeling of Concrete Bubbled Slab, Steel Supporting Plate and Steel loading Plate

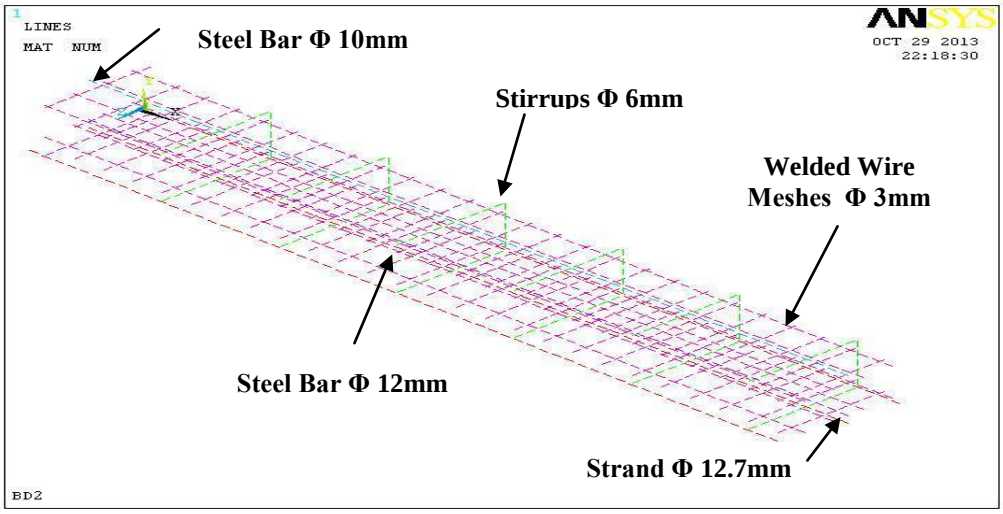

Figure 11. Modeling of Flexural and Shear Reinforcement

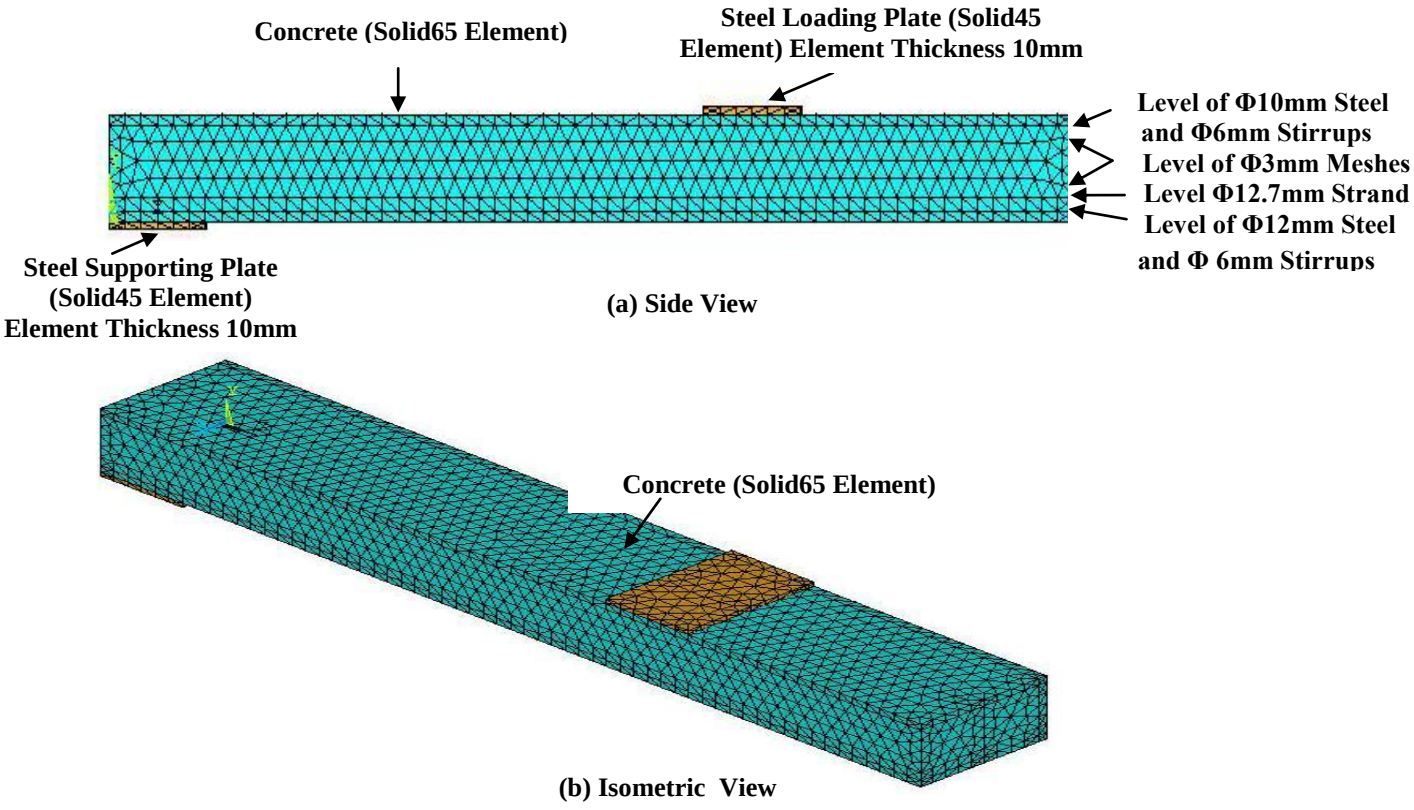

Figure 12. Meshing of Concrete, Support and Plate

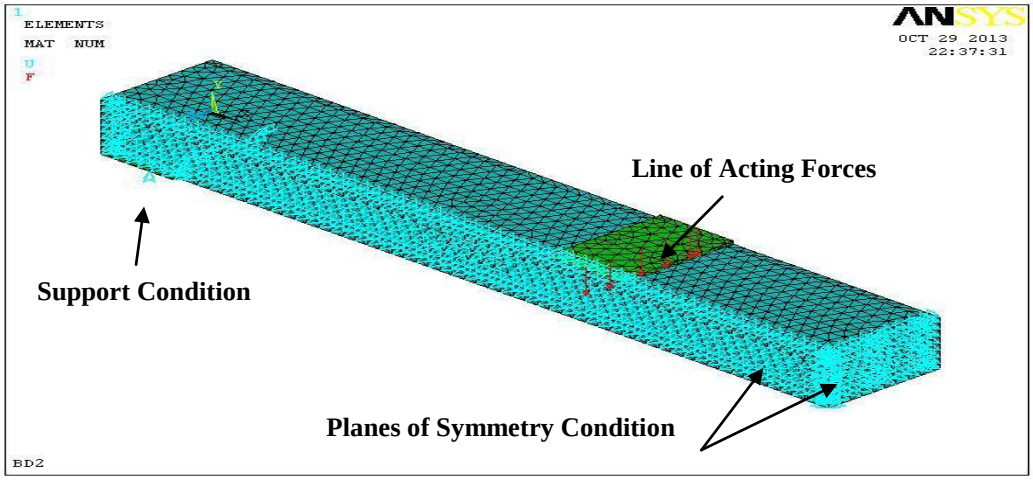

Figure 13. Loads and Boundary Conditions

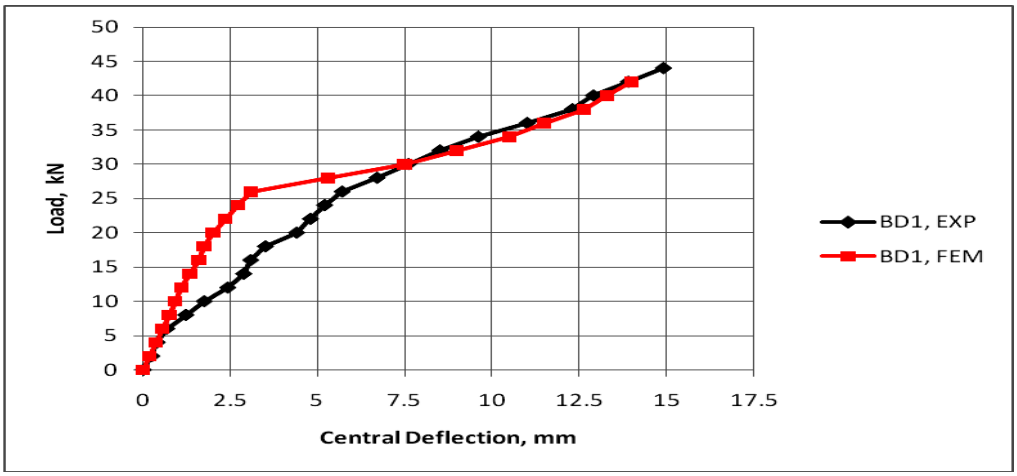

Figure 14. Comparison of Experimental and Analytical Load-Central Deflection Curves for BD1

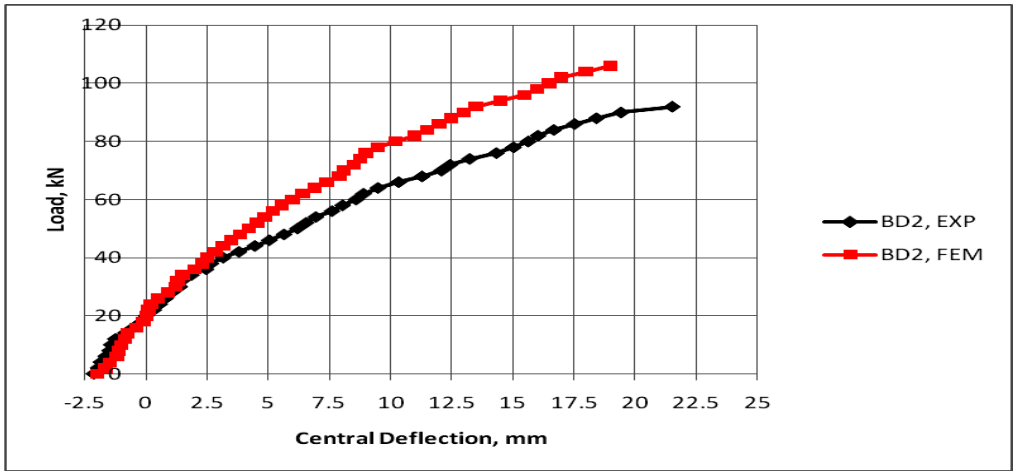

Figure 15. Comparison of Experimental and Analytical Load-Central Deflection Curves for BD2

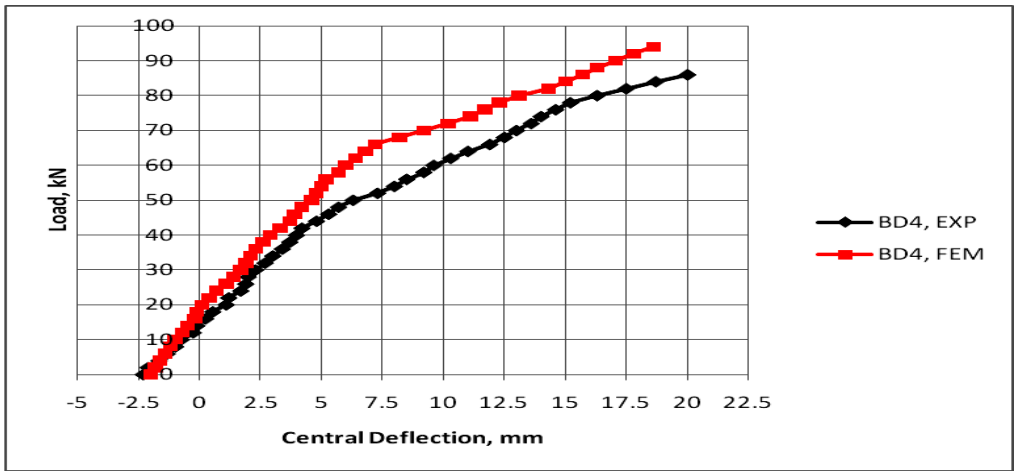

Figure 16. Comparison of Experimental and Analytical Load-Central Deflection Curves for BD4

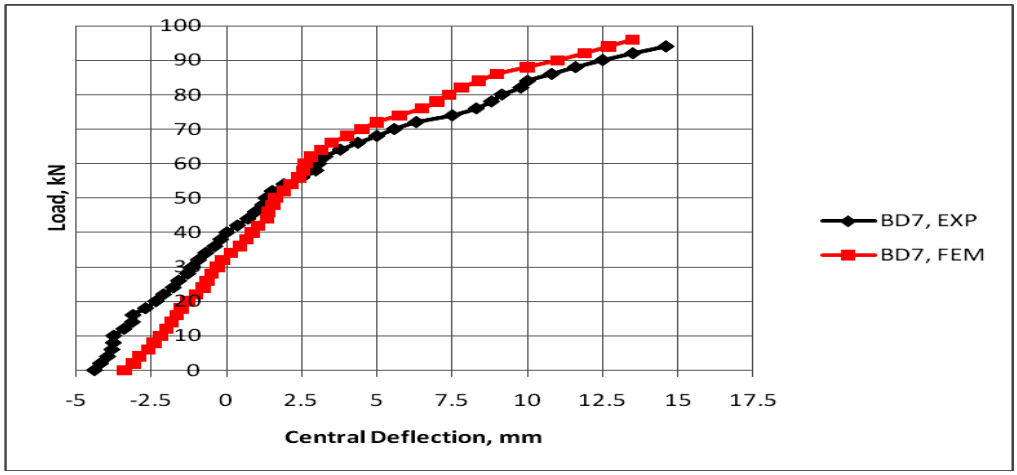

Figure 17. Comparison of Experimental and Analytical Load-Central Deflection Curves for BD7

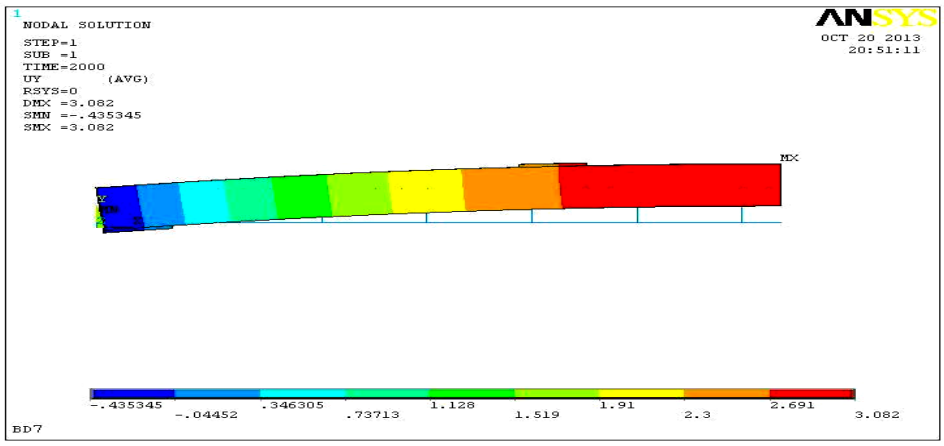

(a) Deflected Shape due to Prestressing Force

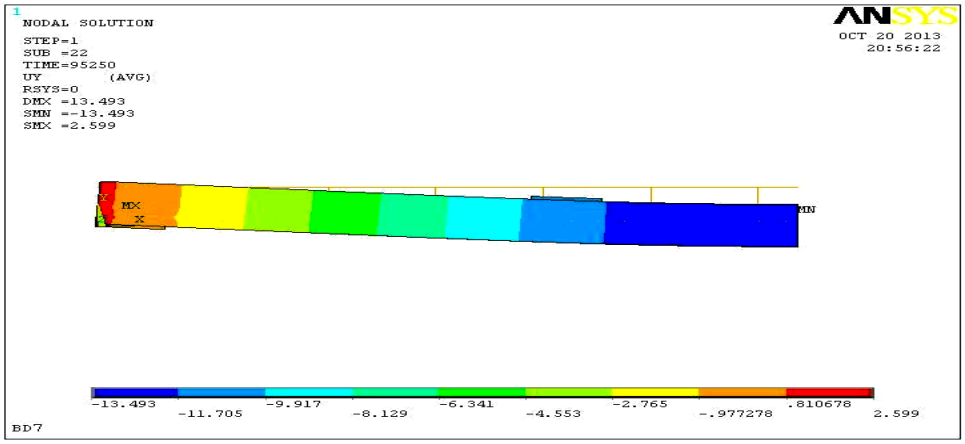

(b) Deflected Shape at Failure

Figure 18. Deflected Shape for BD7

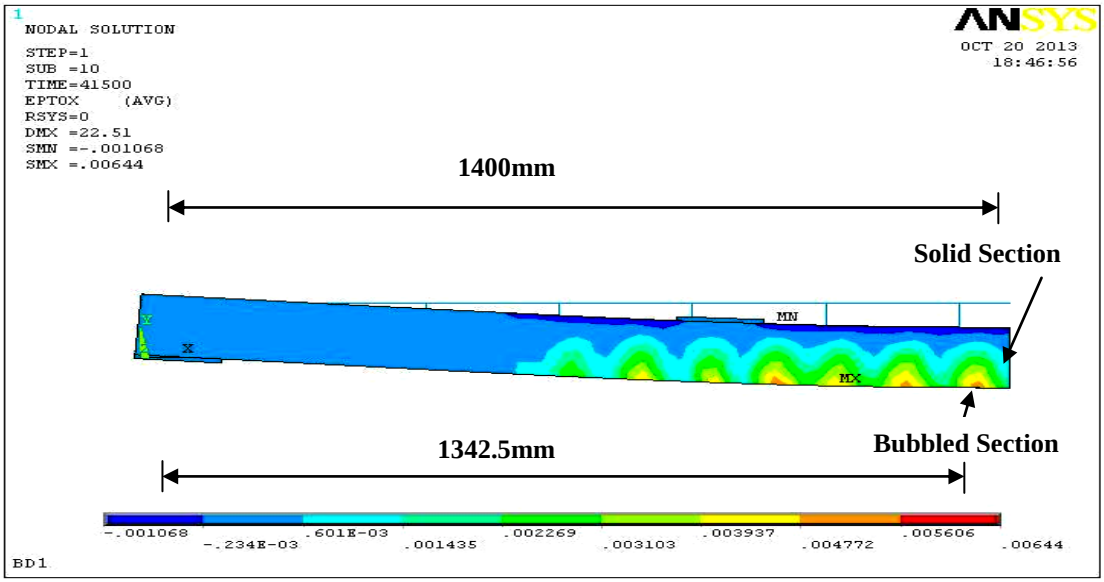

Figure 19. Strain Contour for BD1 at Ultimate Load.

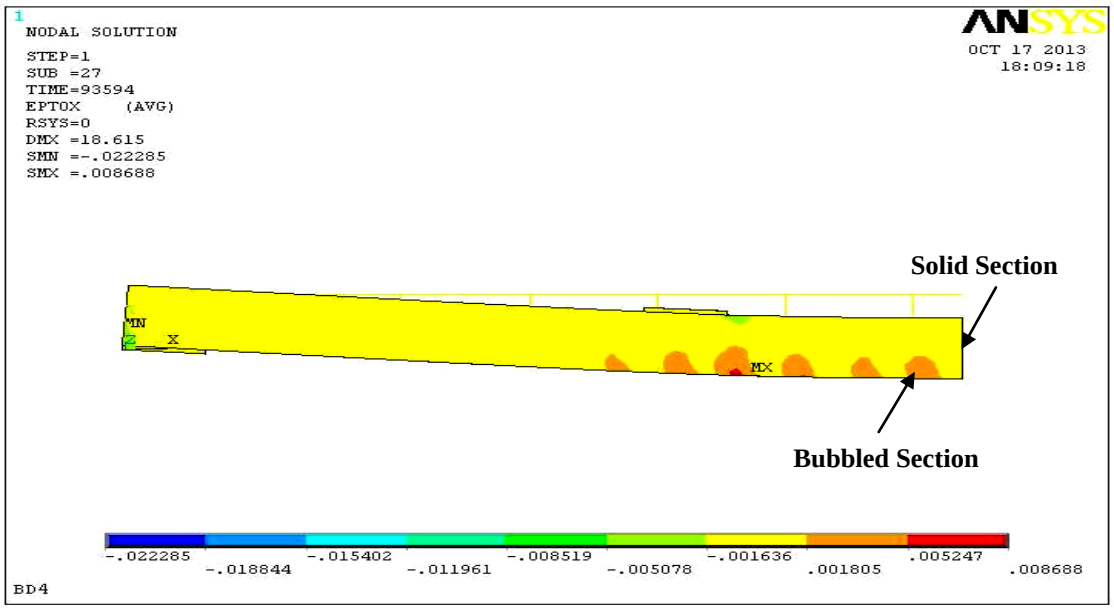

Figure 20. Strain Contour for BD4 at Ultimate Load.

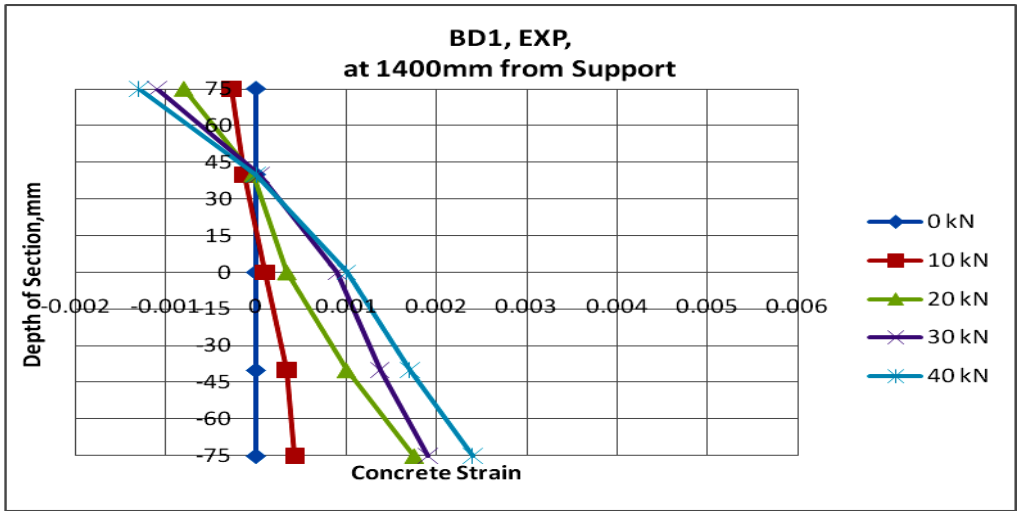

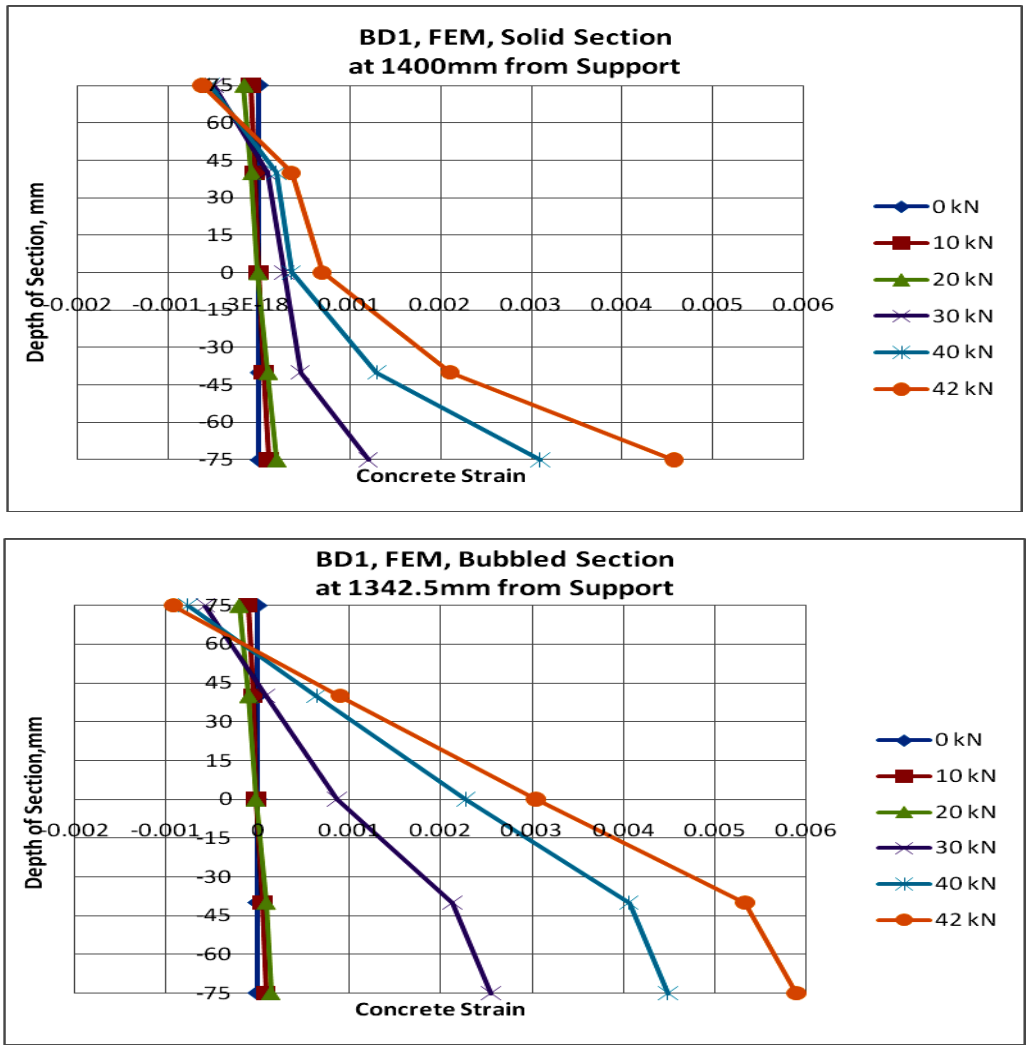

Figure 21. Comparison of Experimental and Analytical Load-Concrete Strain Curves for BD1.

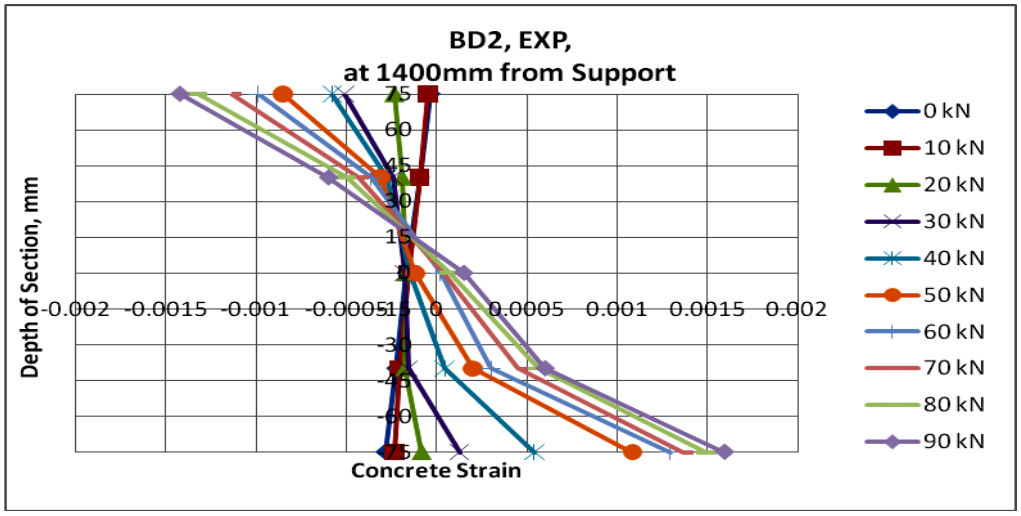

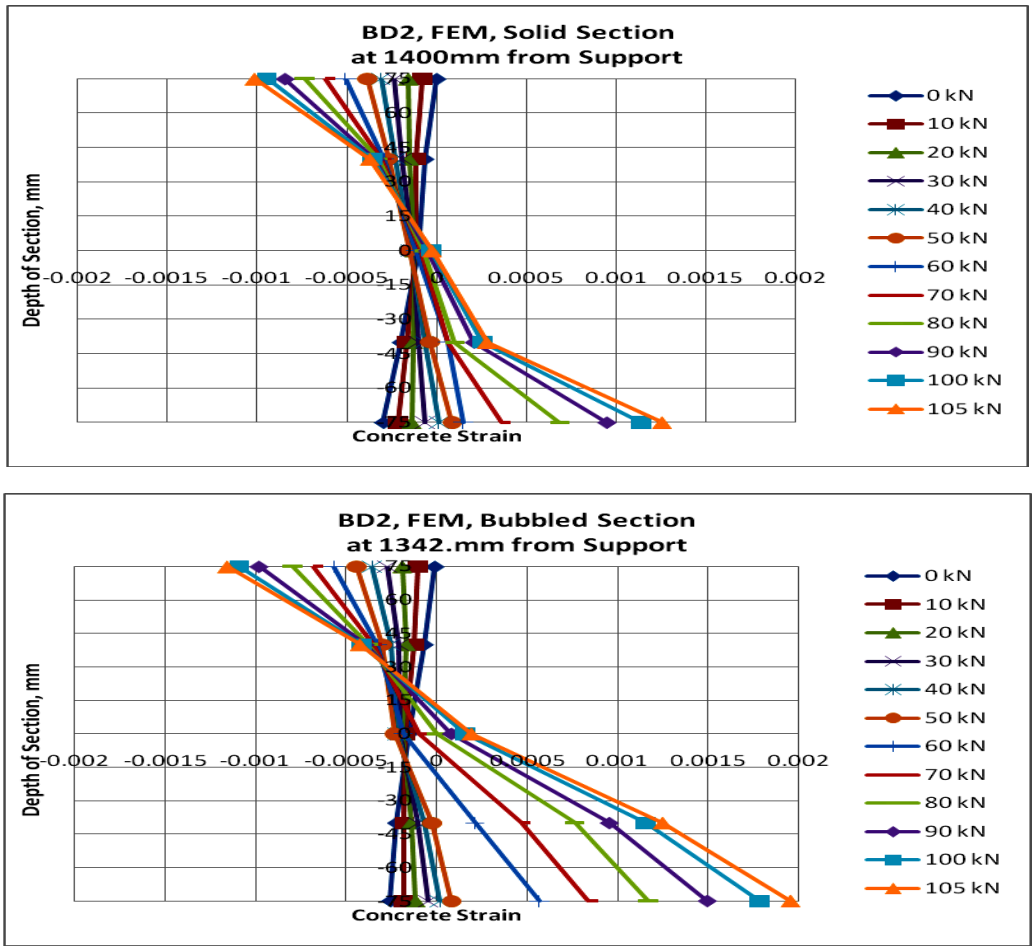

Figure 22. Comparison of Experimental and Analytical Load-Concrete Strain Curves for BD2.

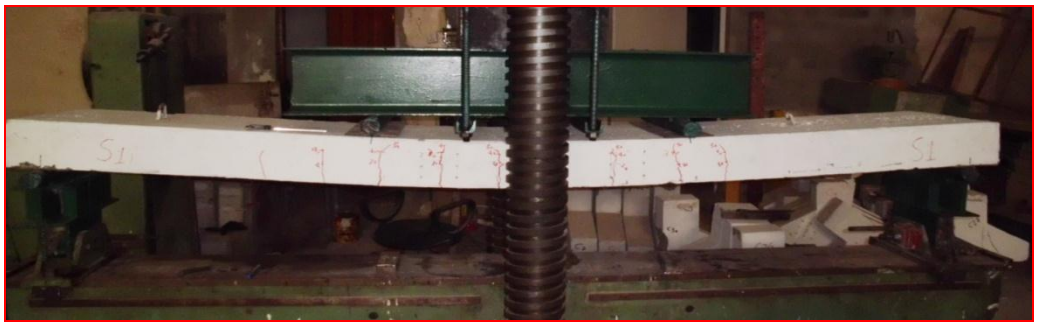

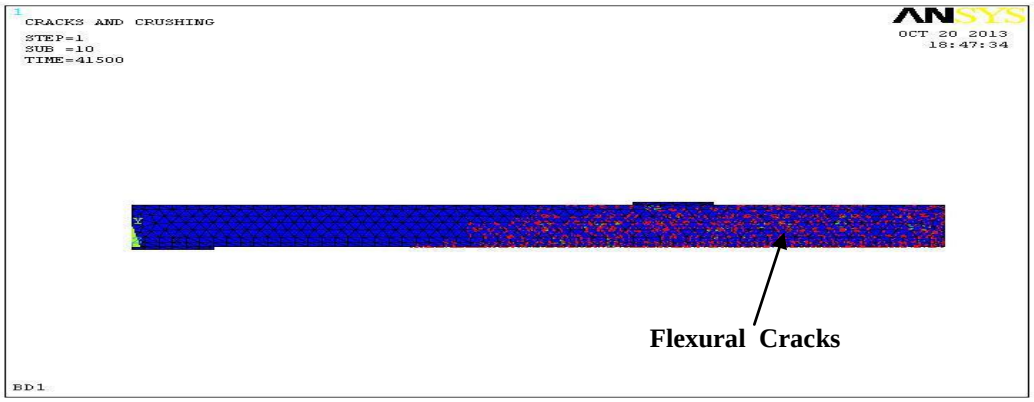

Figure 23. Comparison of Experimental and Analytical Crack Pattern at Ultimate Load for BD1.

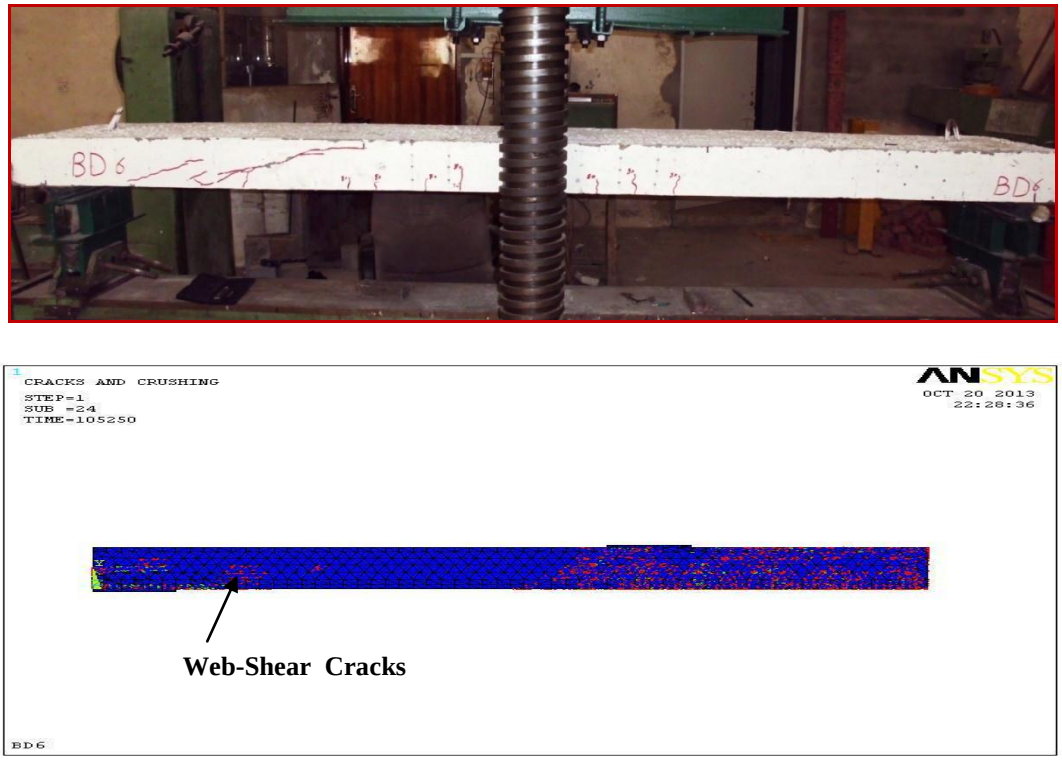

Figure 24. Comparison of Experimental and Analytical Crack Pattern at Ultimate Load for BD6.